

Geological Survey  
of Canada



---

---

## Current Research 2001-E3

# *An analytical procedure for determining spectral induced polarization characteristics of anisotropic rocks, Yellowknife mining district, Northwest Territories*

*T.J. Katsube*

2001

---

---



Natural Resources  
Canada

Ressources naturelles  
Canada

Canada

©Her Majesty the Queen in Right of Canada, 2001  
Catalogue No. M44-2001/E3E  
ISBN 0-660-18586-5

A copy of this publication is also available for reference by depository libraries across Canada through access to the Depository Services Program's website at <http://dsp-psd.pwgsc.gc.ca>

A free digital download of this publication is available from the Geological Survey of Canada Bookstore web site:

<http://gsc.nrcan.gc.ca/bookstore/>

Click on Free Download.

**All requests for permission to reproduce this work, in whole or in part, for purposes of commercial use, resale or redistribution shall be addressed to: Geoscience Information Division, Room 200, 601 Booth Street, Ottawa, Ontario K1A 0E8.**

**Author's address**

*T.J. Katsube (jkatsube@NRCan.gc.ca)  
Mineral Resources Division  
Geological Survey of Canada  
601 Booth Street  
Ottawa, Ontario K1A 0E8*

# An analytical procedure for determining spectral induced polarization characteristics of anisotropic rocks, Yellowknife mining district, Northwest Territories<sup>1</sup>

T.J. Katsube

Mineral Resources Division, Ottawa

*Katsube, T.J., 2001: An analytical procedure for determining spectral induced polarization characteristics of anisotropic rocks, Yellowknife mining district, Northwest Territories; Geological Survey of Canada, Current Research 2001-E3, 11 p.*

---

**Abstract:** Electro-electrochemical models for mineralized rocks previously proposed are generally too simplistic for application to rock textures containing sulphide minerals in anisotropic rocks. A new spectral induced polarization study (1–10<sup>6</sup> Hz) has been carried out to modify and enable application of these models to a typical anisotropic rock with layers enriched in electronically conductive sulphide minerals and layers barren of such minerals. This includes the use of scanning electron microscope images of rocks.

Results indicate the existence of dielectric effects of rock-forming minerals, frequency-dependent permittivity and resistivity effects of pore surfaces in layers barren of sulphides, and nonfrequency-dependent resistivity effects in both the mineralized and nonmineralized layers. Frequency-dependent permittivity effects of electrochemical double layers on sulphide grains in the mineralized layers also existed. These effects have been characterized by nine coefficients of an equivalent circuit to model the rock. These coefficients were determined by interactive curve fitting of calculated to measured curves.

**Résumé :** Les modèles électriques et électrochimiques appliqués aux roches minéralisées, qui ont été jusqu'ici proposés, sont généralement trop simplistes pour que l'on puisse s'en servir pour l'analyse des textures de roches minéralisées en sulfures de caractère anisotrope. Une nouvelle étude de polarisation provoquée spectrale (1-10<sup>6</sup> Hz) a été entreprise dans le but de modifier ces modèles en vue de les appliquer à une roche anisotrope typique se composant de couches enrichies en sulfures électroniquement conducteurs et de couches dépourvues de ces sulfures. Une composante d'imagerie des roches au microscope électronique à balayage fait partie de cette étude.

Les résultats révèlent l'existence d'effets diélectriques de la part des minéraux cardinaux, d'effets de résistivité et de permittivité dépendants de la fréquence au niveau de la surface des pores dans les couches dépourvues de sulfures, ainsi que d'effets de résistivité non dépendants de la fréquence au sein des couches aussi bien minéralisées que non minéralisées. Des effets de permittivité dépendants de la fréquence ont aussi été relevés au niveau de la double couche électrochimique sur les grains de sulfures au sein des couches minéralisées. Ces effets sont représentés par neuf coefficients d'un circuit équivalent agissant comme modèle de la roche. Les valeurs des coefficients ont été déterminés à l'aide d'ajustement interactif des courbes calculées sur les courbes mesurées.

---

<sup>1</sup> Contribution to the 1999-2003 Canada-Northwest Territories Yellowknife Mining Camp Exploration Science and Technology (EXTECH-III) Initiative

## INTRODUCTION

Electro-electrochemical models for mineralized rocks have been proposed since the late 1950s (e.g. Wait, 1959; Ward and Fraser, 1967; Madden and Cantwell, 1967; Dias, 1972; Zonge, 1972; Pelton, 1977; Pelton et al., 1978; Wong, 1979), with many of them summarized in a recent publication (Dias, 2000). The main principles and components of these models are summarized in Figure 1. The model consists of a nonpolarizable electrical current flow path, a flow path interrupted by polarizable electrochemical double layers on the metallic mineral surfaces, and a path influenced by polarizable clay mineral surfaces. The basic principles of the summarized model is adequate, however the model itself is too simplistic for application to actual textures containing electronically conductive minerals in anisotropic rocks. In addition, it lacks the dielectric effect of rock-forming minerals which enter at the higher frequencies (e.g. Katsube and Collett, 1975; Katsube, 1975a). A scanning electron microscope (SEM) image of a typical anisotropic rock with layers of enriched sulphide minerals is displayed in Figure 2 (Connell et al., 2000). In the direction parallel to the layers, this rock consists of two types of electrical conductors (T.J. Katsube, J. Mwenifumbo, J. Kerswill, S. Connell, and N. Scromeda-Perez, online, [http://www.nrcan.gc.ca/gsc/mrd/extech3/2000\\_geo\\_forum\\_e.html](http://www.nrcan.gc.ca/gsc/mrd/extech3/2000_geo_forum_e.html)), one of electrical conductivity through the pore-fluid system,

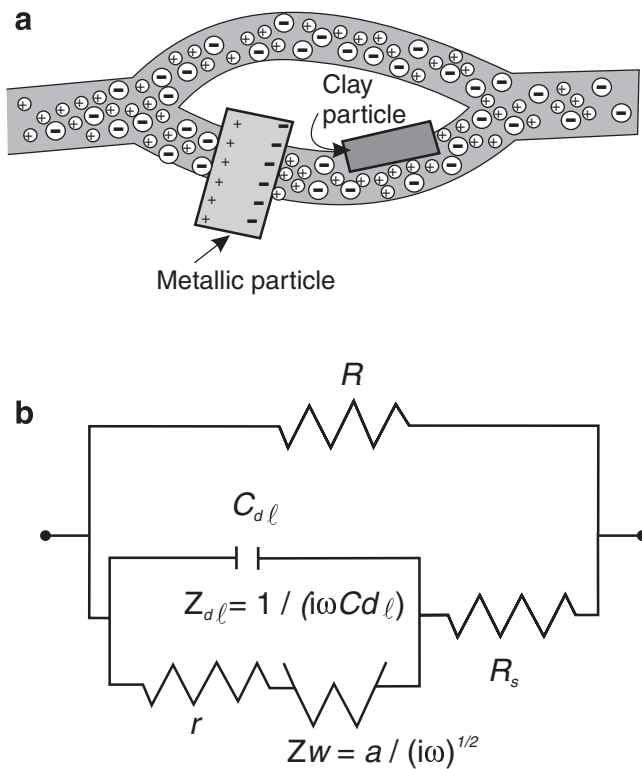


**Figure 1.** Main principles of the electro-electrochemical models commonly used for **a)** mineralized rocks and **b)** their equivalent circuit (Dias, 2000).

and the other of electrical conductivity through pore fluid short-circuited by electronic conductors. At the higher frequencies the layers containing the electronically conductive sulphide mineral grains will contribute to reduced bulk resistivity of the rock due to the frequent short-circuits caused by these grains. At lower frequencies, however the electrical current flow paths in these mineralized layers will be disrupted by electrochemical double layers on the conductive mineral surfaces becoming charged and acting as electrical insulators. This will result in the main electrical conductivity path shifting from the layers containing conductive grains to the layers barren of these grains (T.J. Katsube, J. Mwenifumbo, J. Kerswill, S. Connell, and N. Scromeda-Perez, online, [http://www.nrcan.gc.ca/gsc/mrd/extech3/2000\\_geo\\_forum\\_e.html](http://www.nrcan.gc.ca/gsc/mrd/extech3/2000_geo_forum_e.html)). The frequency at which this occurs will have significant implications on mineral exploration strategies.

This paper discusses the electrical theories and rock elements involved in the transition of these electrical current flow paths, and the methods for analysis using measured results for an anisotropically mineralized rock from the Yellowknife mining district (Connell et al., 2000; Scromeda et al., 2000), Northwest Territories.

## THEORY

### Equivalent circuit and parameters of an anisotropic mineralized rock sample

The equivalent circuit proposed for an anisotropic mineralized rock in Figure 2 is shown in Figure 3. It is a modification of those proposed by Ward and Fraser (1967) and Dias (1972, 2000). The C<sub>D</sub> represents the capacitance due to the dielectric characteristics of the entire rock sample and R<sub>P</sub> represents the resistance to the electrical current flowing through the pores of the nonmineralized layer of the sample. The R<sub>S</sub>ω<sup>-α<sub>SR</sub></sup> and C<sub>S</sub>ω<sup>-α<sub>SC</sub></sup> represent the frequency-dependent resistance and capacitance effects of the pore surfaces in the nonmineralized layer, respectively, where α<sub>SR</sub> and α<sub>SC</sub> are coefficients and ω is the angular frequency. The R<sub>M</sub> and C<sub>M</sub>ω<sup>-α<sub>M</sub></sup> are the resistance to the electrical current flowing through the pores of the conductive mineral grains and the frequency-dependent capacitance of the electrochemical double layers on the surfaces of these conductive grains, respectively, where α<sub>M</sub> is a coefficient.

The admittances (Y<sub>1</sub>, Y<sub>2</sub>, and Y<sub>3</sub>) of the top three arms of the equivalent circuit (Fig. 3) are

$$Y_1 = j\omega C_D, \quad (1)$$

$$Y_2 = 1/R_P, \quad (2)$$

$$Y_3 = 1/(R_S\omega^{-\alpha_{SR}}) + jC_S\omega^{1-\alpha_{SC}}, \quad (3)$$

where

$$j = \sqrt{-1}, \quad (4)$$

$$\omega = 2\pi f, \quad (5)$$

## Sericite schist sample MYG-11a (BSEI)

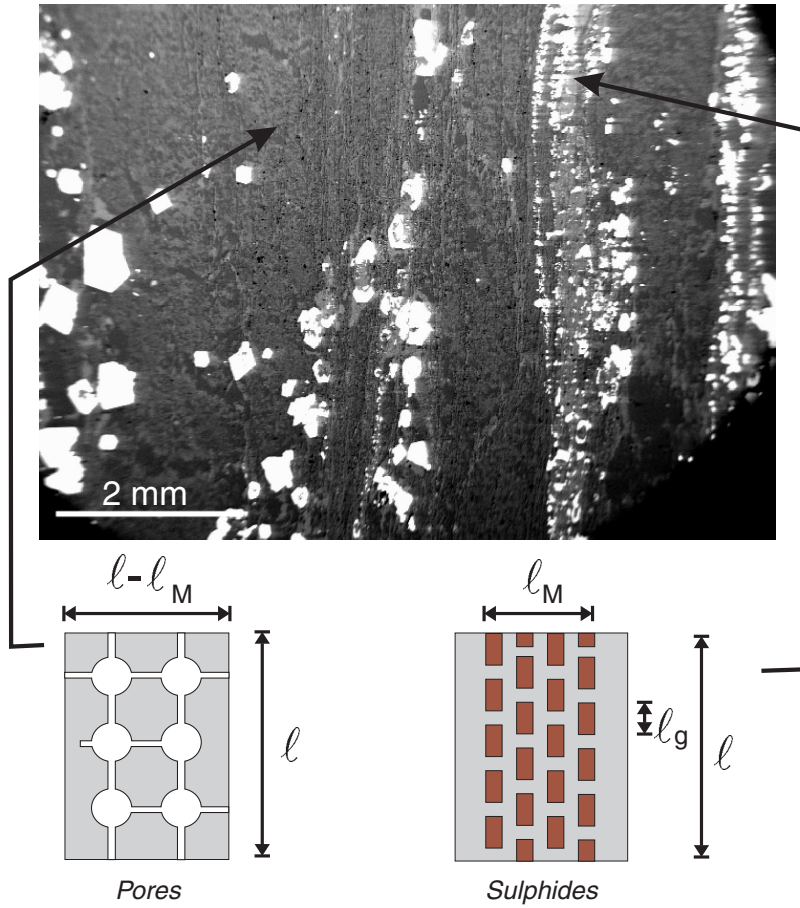


**Figure 2.**

Scanning electron microscope (SEM) image of a typical anisotropic rock (sericite schist, Northwest Territories) with layers of enriched sulphide mineral content (Connell et al., 2000). The rock consists of two types of electrical conductors (T.J. Katsube, J. Mwenifumbo, J. Kerswill, S. Connell, and N. Scromeda-Perez, online, [http://www.nrcan.gc.ca/gsc/mrd/extech3/2000\\_geo\\_forum\\_e.html](http://www.nrcan.gc.ca/gsc/mrd/extech3/2000_geo_forum_e.html)), one of electrical conductivity through the pore-fluid system, and the other of electrical conductivity through pore-fluid short-circuited by electronic conductors (sulphide minerals).

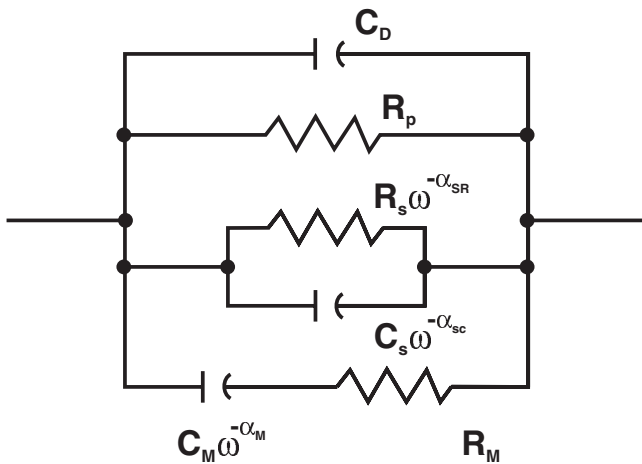


**Figure 3.** Equivalent circuit of the anisotropic mineralized rock (Fig. 2). The  $C_D$  is the capacitance due to the dielectric characteristics of the rock,  $R_P$  is the resistance to the electrical current flow through the pores of the nonmineralized layer, and  $R_S \omega^{-\alpha_{SR}}$  and  $C_S \omega^{-\alpha_{SC}}$  are the frequency-dependent resistance and capacitance of the pore surfaces in the nonmineralized layer, where  $\alpha_{SR}$  and  $\alpha_{SC}$  are coefficients and  $\omega$  is the angular frequency. The  $R_M$  and  $C_M \omega^{-\alpha_M}$  are the resistance and frequency-dependent capacitance of the mineralized layers, where  $\alpha_M$  is a coefficient.

and where  $f$  is the frequency of measurement. Since the impedance ( $Z_4$ ) of the fourth arm of the equivalent circuit is

$$Z_4 = R_M - j/(C_M \omega^{1-\alpha_M}), \quad (6)$$

the admittance of this arm is

$$Y_4 = 1/Z_4 = \tau^2 / \{R_M(\tau^2 + 1)\} + j\tau / \{R_M(\tau^2 + 1)\}, \quad (7)$$

where  $\tau$  is the time constant of that arm:

$$\tau = R_M C_M \omega^{1-\alpha_M}. \quad (8)$$

The complex admittance ( $Y^*$ ) of this circuit is,

$$Y^* = Y' + jY'' = Y_1 + Y_2 + Y_3 + Y_4, \quad (9)$$

$$Y^+ = \sqrt{(Y')^2 + (Y'')^2}, \quad (10)$$

where  $Y'$ ,  $Y''$ , and  $Y^+$  are the real admittance, imaginary admittance, and amplitude or absolute value of complex admittance, respectively. From Equations (1), (2), (3), (7), (8), and (9) we obtain

$$Y' = 1/R_P + 1/(R_S \omega^{-\alpha_{SR}}) + \tau^2 / \{R_M(\tau^2 + 1)\}, \quad (11)$$

$$Y'' = \omega C_D + C_S \omega^{1-\alpha_{SC}} + \tau / \{R_M(\tau^2 + 1)\}. \quad (12)$$

The complex impedance ( $Z^*$ ), real impedances ( $Z'$ ), and imaginary impedance ( $Z''$ ) of the entire rock sample are related to  $Y^*$ ,  $Y'$ , and  $Y''$  by

$$Z^* = 1/Y^*, \quad (13)$$

$$Z' = Y' / (Y^+)^2, \quad (14)$$

$$Z'' = Y'' / (Y^+)^2, \quad (15)$$

where

$$Z^* = Z' - jZ'', \quad (16)$$

and where  $Z^+$  is the amplitude or absolute value of complex impedance,

$$Z^+ = \sqrt{(Z')^2 + (Z'')^2}. \quad (17)$$

### Complex resistivity and complex conductivity equations

The complex resistivity ( $\rho^*$ ) and complex conductivity ( $\sigma^*$ ) equations are as follows:

$$\rho^* = \rho' - j\rho'', \quad (18)$$

$$\rho^+ = \sqrt{(\rho')^2 + (\rho'')^2}, \quad (19)$$

$$\sigma^* = 1/\rho^* = \sigma' + j\sigma'', \quad (20)$$

$$\sigma^+ = \sqrt{(\sigma')^2 + (\sigma'')^2}. \quad (21)$$

where  $\rho'$ ,  $\rho''$  and  $\rho^+$  are the real resistivity, imaginary resistivity, and amplitude of the complex resistivity, respectively, and  $\sigma'$ ,  $\sigma''$  and  $\sigma^+$  are the real conductivity, imaginary conductivity, and amplitude of the complex conductivity of the sample, respectively. Similar to Equations (14) and (15)

$$\sigma' = \rho' / (\rho^+)^2, \quad (22)$$

$$\sigma'' = \rho'' / (\rho^+)^2. \quad (23)$$

These are related to  $Y^*$  and  $Z^*$  by (von Hippel, 1954a, b)

$$Z^* = \rho^* / K_G = (\rho' - j\rho'') / K_G, \quad (24)$$

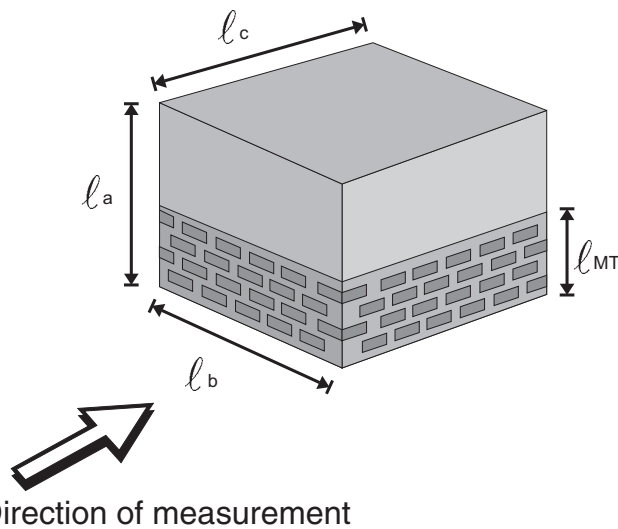


**Figure 4.** Diagram showing the geometry of the sample used in this study, and the definition of geometric factor ( $K_G$ ):  $K_G = l_a l_b / l_c$ , where  $l_a$ ,  $l_b$ , and  $l_c$  are the dimensions of the rectangular sample. The mineralized and nonmineralized layers have thicknesses of  $l_{MT}$  and  $l_b - l_{MT}$ , respectively.

$$Y^* = K_G \sigma^* = K_G (\sigma' + j\sigma''). \quad (25)$$

The  $K_G$  is the geometric factor defined by

$$K_G = l_a l_b / l_c, \quad (26)$$

where  $l_a$ ,  $l_b$ , and  $l_c$  represent the dimensions of the rectangular sample as shown in Figure 4. The  $l_c$  represents the length of the sample in the direction of measurement or the direction parallel to foliation in this case, and  $l_a$  and  $l_b$  represent the lengths of the sample perpendicular to measurement. In cases where the characteristics of the individual layers need to be considered, thicknesses of the mineralized ( $l_{MT}$ ) and nonmineralized ( $l_b - l_{MT}$ ) layers will have to be used in the geometric factor value determinations.

## ANALYTICAL APPROACH

### Sample

The sample used in this study is an electrically anisotropic sericite schist (sample number MYG-11A) from the Yellowknife mining district, Northwest Territories (Connell et al., 2000). It is rectangular with the dimensions listed in Table 1 (Scromeda et al., 2000) and the bulk electrical resistivity ( $\rho_R$ ) values in the three directions shown in Figure 5 (Connell et al., 2000). It describes the higher  $\rho_R$  values are in the  $\alpha$ -direction perpendicular to foliation. The method used to determine the  $\rho_R$  values using the Cole-Cole or argon diagrams (Katsube and Mareschal, 1993) are also shown in this figure. Further details of this method are described elsewhere (e.g. Scromeda et al., 2000).

### Sample holder and measuring system

The sample holder and measuring system used to obtain these data have been frequently described elsewhere (e.g. Katsube, 1975b, c; Gauvreau and Katsube, 1975; Katsube and Walsh, 1987; Katsube and Salisbury, 1991). The sample holder is a two-electrode system with stainless steel electrodes but with graphite plates placed between these electrodes and the sample, as shown in Figure 6a. The equivalent circuit of this system is shown in Figure 6b. The  $C_E$  represents the electrode capacitance which, in this case, is that of the graphite plates since they are in direct contact with the sample. The stray and

**Table 1.** Geometric and some petrophysical characteristics of the electrically anisotropic sericite schist sample (MYG-11A, Yellowknife mining district, Northwest Territories) that was used in this study (Scromeda et al., 2000).

Parameter	Symbol	Value	Units
Geometrical dimensions	$l_a$	1.51	cm
	$l_b$	2.14	cm
	$l_c$	2.17	cm
Geometric factor	$K_G$	$1.49 \times 10^{-2}$	m
Bulk density	$\delta_G$	3.04	g/mL
Bulk electrical resistivity ( $\beta$ -direction)	$\rho_r$	360	$\Omega m$

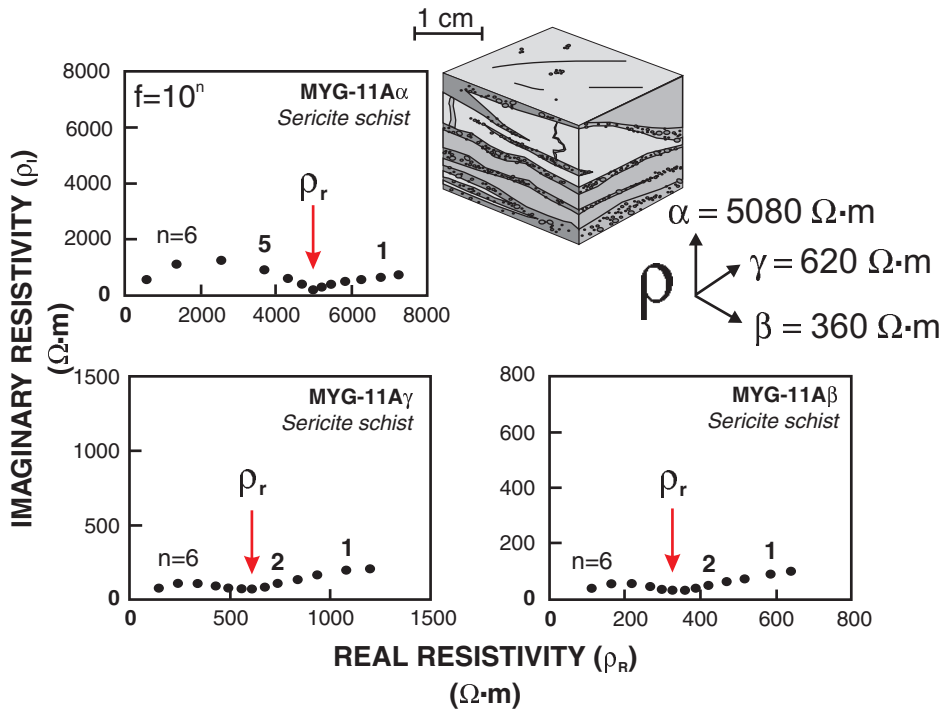
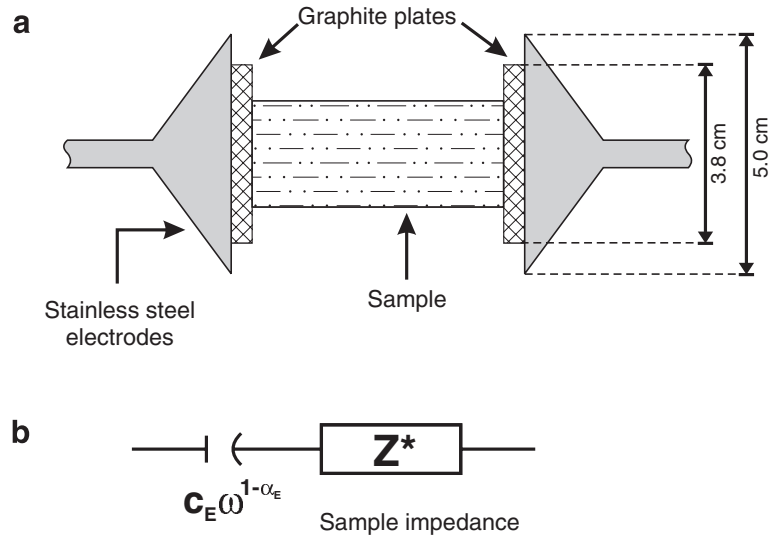


**Figure 5.**

Description of the sericite schist sample used in this study (sample number MYG-11A) from the Yellowknife mining district, Northwest Territories (Connell et al., 2000), with the bulk electrical resistivity ( $\rho_R$ ) values shown in the three directions. The foliation is generally in the  $\beta$ - and  $\gamma$ -directions.

**Figure 6.**

The **a)** two-electrode sample holder system, used in this study, with stainless steel electrodes but with graphite plates placed between the electrodes and the sample, and the **b)** equivalent circuit of this system (Gauvreau and Katsube, 1975; Katsube and Collett, 1975).  $C_E$  is the electrode capacitance (graphite plate).



leakage capacitances of the sample holder system are eliminated at the time of measurement (Katsube and Collett, 1973; Gauvreau and Katsube, 1975).

### Sample data

The data used in this study are for the  $\beta$ -direction (Fig. 5) of sample MYG-11A, and has previously been published (Table 2). This data includes the effect of the capacitance ( $C_E$ ) of the electrochemical double layers on the electrodes (graphite plates). Therefore, this effect will have to be eliminated prior to data analysis. Since the impedance and reactance of the sample and electrodes are  $Z^*$  and  $X_E$ , respectively, the impedance of the sample-electrode package ( $Z_{MS}$ ) is

$$Z_{MS} = -jX_E + Z^*, \quad (27)$$

where

$$X_E = 1/(C_E \omega^{1-\alpha_E}), \quad (28)$$

and where  $\alpha_E$  is a coefficient. Results of recent tests performed to determine the characteristics of the graphite electrodes (diameter: 3.8 cm) used in these measurements indicate that

$$C_E = 2.1 \times 10^{-3} \text{ (farads)}, \quad (29)$$

$$\alpha_E = 0.45. \quad (30)$$

The electrode characteristics may change slightly from measurement to measurement, due to wearing and contamination of the electrode surfaces and the chemical characteristics of

**Table 2.** Measured\*\* apparent complex resistivity data for the  $\beta$ -direction of the electrically anisotropic sericite schist sample, MYG-11A, from the Yellowknife mining district, Northwest Territories (Scromeda et al., 2000).

f	$\rho^+$	$\rho'$	$\rho''$	D	$\Delta\rho^+$
1	649	641	102	6.3	8.8
3	592	585	90.8	6.4	11.9
10	521	516	75.4	6.8	8.8
30	475	471	63.9	7.4	10.9
$10^2$	423	420	49.6	8.5	7.8
$3 \times 10^2$	390	388	39.6	9.8	7.8
$10^3$	360	359	32.0	11.2	8.8
$3 \times 10^3$	328	327	34.2	9.5	8.8
$10^4$	299	297	38.1	7.8	9.8
$3 \times 10^4$	270	266	47.3	5.6	16.6
$10^5$	225	218	57.6	3.8	22.7
$3 \times 10^5$	174	164	57.2	2.9	32.0
$10^6$	118	111	41.2	2.7	
Hz	$\Omega\text{m}$	$\Omega\text{m}$	$\Omega\text{m}$		(%)

f = Frequency  
 $\rho^+$  = Amplitude of measured\*\* complex resistivity  
 $\rho'$  = Real resistivity  
 $\rho''$  = Imaginary resistivity  
D = Loss  
 $\Delta\rho^+$  = Complex resistivity gradient  
\*\* = Measured, in this case, implies that the results are of the sample and sample-holder system

the solutions in the rock sample under test. Nevertheless, the values in Equation (29) and (30) should present a good estimate of the actual  $C_E$  values in a measurement.

**Analytical procedure**

The first step in this analysis is to determine  $Z^+$ ,  $Z'$ , and  $Z''$  from the published complex resistivity values of  $\rho^+$ ,  $\rho'$ , and  $\rho''$  in Table 2. This is accomplished by dividing the complex resistivity values by the geometric factor ( $K_G$ , Table 1). That is, from Equations (27), (28), and (24), we obtain data represented by

$$Z_{MS} = -j/(C_E \omega^{1-\alpha_E}) + (\rho' - j\rho'')/K_G \quad (31)$$

The second step of the analysis is to eliminate the electrode effect from the measured data using Equations (31), (29), and (30). The published complex resistivity values in Table 2 are actually apparent values, since the electrode effect has not been eliminated.

**ANALYTICAL RESULTS**

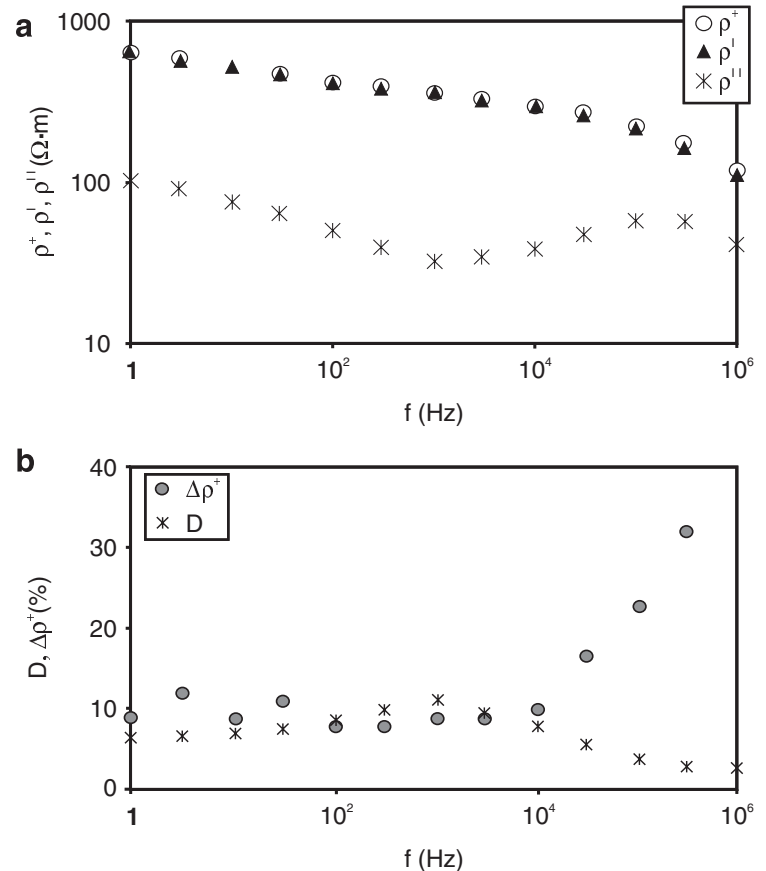
**Electrode effects**

The apparent complex resistivity ( $\rho^*$ ) curves for sample MYG-11A, used in this study, are shown in Figure 7. The loss (D) and complex resistivity gradient ( $\Delta\rho^+$ ) data are also included in this figure:

$$D = \rho'/\rho'' = \sigma'/\sigma'' \quad (32)$$

**Figure 7.**

Complex resistivity ( $\rho^*$ ) curves for sample MYG-11A (Scromeda et al., 2000), used in this study. D and  $\Delta\rho^+$  are the loss (Equation 32) and resistivity gradient (Equation 33), respectively. The  $\rho^+$  is the amplitude of the complex resistivity.





$$\Delta\rho^+ = (\Delta\rho^+_i - \Delta\rho^+_{i+1})/\Delta\rho^+_i, \quad (33)$$

where  $i$  and  $i+1$  represent the frequency and adjacent frequency (e.g. 10 and 30 Hz or 300 and 1000 Hz) at which these measurements were taken. The published data in Table 2 were converted into complex impedance ( $Z^*$ ) and complex admittance ( $Y^*$ ) data in Table 3 using Equations (16) and (24), and then Equations (14) and (15). A geometric factor value ( $K_G$ ) of  $1.49 \times 10^{-2}$  (Table 1) was used in these conversions. The  $Z^+$  and  $Z''$  data are plotted in Figure 8. Included in the figure is the curve for the electrode reactance ( $X_E$ ). The

electrode capacitance of  $2.1 \times 10^{-3}$  F in Equation (27) is for a graphite disc with an area of  $11.3 \text{ cm}^2$ , whereas the actual contact space with the sample is only  $3.23 \text{ cm}^2$  (Table 1). Accordingly, the electrode capacitance value used in the determination of  $X_E$  (Fig. 8) has been reduced to  $6.01 \times 10^{-4}$  F. As shown in Figure 8, the maximum  $X_E$  value for the frequency range used in this study is  $601 \Omega$  (1.0 Hz), a value less than 9% of that of  $Z''$  at 1.0 Hz. Therefore, the current electrode effects are considered negligible in this study.

### Coefficient and parameter estimates

Several methods have been used for the initial estimates of the equivalent circuit coefficients (Fig. 3). For the capacitance ( $C_D$ ) of the rock sample (Equation 1), a dielectric constant ( $\kappa$ ) of 10 was used since the sample is disseminated with metallic sulphide minerals and the value of  $C_D$  estimated by using the following equation:

$$C_D = \kappa \epsilon_0 K_G, \quad (34)$$

where  $\epsilon_0$  is the permittivity of vacuum ( $8.854 \times 10^{-12}$  F/m). The result is listed in Table 4.

The real ( $Y'$ ) and imaginary ( $Y''$ ) admittance versus frequency ( $f$ ) curves are displayed in Figures 9a and 9b for sample MYG-11A. The open circles represent the actual measured data points. Estimates from previous studies (Katsube, 1975a, b, c) suggest that  $C_D$  and  $C_M$  are in the ranges of  $10^{-12}$ – $10^{-10}$  F and  $10^{-6}$ – $10^{-4}$  F, respectively, and that  $C_S$  takes a value between these two ranges. Based on these studies, let us assume that the relationship between the three capacitances in Equations (11) and (12) are

$$C_D \ll C_S \ll C_M.$$

In addition, let us assume that at the higher frequencies (e.g.  $f > 1000$  Hz) it is considered that  $\tau \gg 1$  (Equation 8). Under these assumptions, Equations (11) and (12) representing the  $Y'$ - $f$  and  $Y''$ - $f$  curves, can be replaced by the following two equations:

$$Y' = 1/R_P + 1/(R_S \omega^{-\alpha_{SR}}) + 1/R_M, \quad (35)$$

$$Y'' = \omega C_D + C_S \omega^{1-\alpha_{SC}}. \quad (36)$$

Again, based on these assumptions, a linear section of the curve was selected to determine the values of  $C_S$  and  $\alpha_{SC}$  (Equation 36) at the higher frequencies ( $> 10^4$  Hz) of the  $Y''$ - $f$  curve (Fig. 9b). Linear regression analysis was applied, using the reduced major

**Table 3.** Complex impedance and admittance data obtained from the complex resistivity data for the  $\beta$ -direction of the electrically anisotropic sericite schist sample MYG-11A in Table 2.

f	$Z^+ (x10^4)$	$Z' (x10^4)$	$Z'' (x10^3)$	$Y^+ (x10^{-6})$	$Y' (x10^{-6})$	$Y'' (x10^{-6})$
1	4.36	4.30	6.83	22.9	22.7	3.60
3	3.97	3.92	6.09	25.2	24.9	3.86
10	3.50	3.46	5.06	28.6	28.3	4.14
30	3.19	3.16	4.29	31.4	31.1	4.21
$10^2$	2.84	2.82	3.33	35.2	35.0	4.12
$3 \times 10^2$	2.62	2.61	2.66	38.2	38.0	3.87
$10^3$	2.42	2.41	2.15	41.4	41.2	3.68
$3 \times 10^3$	2.20	2.19	2.30	45.4	45.1	4.73
$10^4$	2.01	1.99	2.55	49.8	49.4	6.33
$3 \times 10^4$	1.81	1.78	3.18	55.2	54.3	9.67
$10^5$	1.51	1.46	3.87	66.2	64.0	16.9
$3 \times 10^5$	1.17	1.10	3.84	85.6	80.8	28.1
$10^6$	0.795	0.745	2.77	132.0	118	43.8
Hz	$\Omega$	$\Omega$	$\Omega$	S	S	S

$Z^+$  = Amplitude of complex impedance  
 $Z'$  = Real impedance  
 $Z''$  = Imaginary impedance  
 $Y^+$  = Amplitude of complex admittance  
 $Y'$  = Real admittance  
 $Y''$  = Imaginary admittance

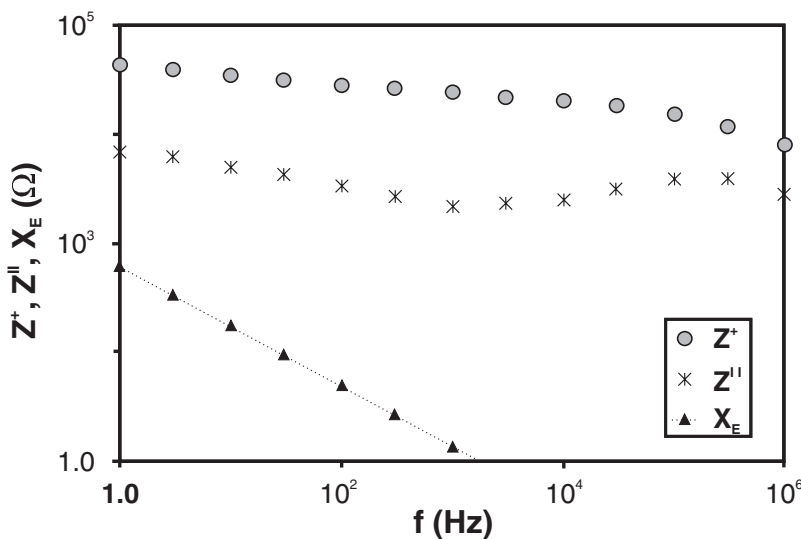


**Figure 8.** Amplitude of complex impedance ( $Z^+$ ) and imaginary impedance ( $Z''$ ) curves for the sample used in this study, with the electrode impedance ( $Z_E''$ ) curve shown at the lower left hand section of the diagram.

axis method (Davis, 1986). Similarly, the values of  $R_S$  and  $\alpha_{SR}$  (Equation 35) were determined from the  $Y'$ - $f$  curve (Fig. 9a), at similar frequencies ( $>10^5$  Hz).

At the lower frequency end (e.g.  $f < 10-300$  Hz), let us consider  $\tau \ll 1$  (Equation 8), so that Equations (11) and (12) can be replaced by the following two equations:

$$Y' = 1/R_P + R_M(C_M\omega^{1-\alpha_M})^2, \quad (37)$$

$$Y'' = C_M\omega^{1-\alpha_M}. \quad (38)$$

Based on these considerations, the values of  $C_M$  and  $\alpha_M$  have been estimated from the lower frequency end of the  $Y''$ - $f$  curve (Fig. 9b), using Equation (38). Knowing the value of  $C_M$ , the value of  $R_M$  was estimated by the same method at these frequencies, using Equation (37). Again, knowing the values of  $C_M$ ,  $\alpha_M$ , and  $R_M$  in Equation (37),  $R_P$  was calculated from a  $Y'$  value at the very lower frequency end of the  $Y'$ - $f$  curve (Fig. 9a). The results of these initial estimates and the frequency ranges of sections of the curves used are listed in Table 4. All of the correlation factor ( $r$ ) values of these linear regression analyses were larger than 0.994, so that the error ranges were negligible and not listed in the table.

**Table 4.** Equivalent circuit coefficients in Equation (1) to (6) determined by several methods, including curve fitting of the measured complex admittance data in Table 3 and Figures 9a and 9b.

Coefficients / parameters	Symbols	Initial values	Frequency range (Hz)	Final values	Error	Units
Capacitance of rock sample	$C_D$	$1.3 \times 10^{-12}$		$2 \times 10^{-12}$	$\pm 50\%$	F
Capacitance of pore surfaces	$C_S$	$5.46 \times 10^{-8}$	$10^4-10^6$	$6 \times 10^{-8}$	$\pm 20\%$	F
Coefficient	$\alpha_{SC}$	0.571	$10^4-10^6$	0.59	$\pm 1\%$	
Resistance of pore surfaces	$R_S$	$5.72 \times 10^5$	$10^5-10^6$	$1.2 \times 10^6$	$\pm 5\%$	$\Omega$
Coefficient	$\alpha_{SR}$	0.268	$10^5-10^6$	0.3	$\pm 12\%$	
Resistance of nonmineralized layer	$R_P$	$7.4 \times 10^4$		$5 \times 10^4$	$\pm 20\%$	$\Omega$
Capacitance of mineralized layer	$C_M$	$3.22 \times 10^{-6}$	1-10	$1.95 \times 10^{-6}$	$\pm 40\%$	F
Coefficient	$\alpha_M$	0.959	1-10	0.596	$\pm 8\%$	
Resistance of mineralized layer	$R_M$	$1.85 \times 10^6$	$1-3 \times 10^2$	$10^5$	$\pm 15\%$	$\Omega$

F = farads

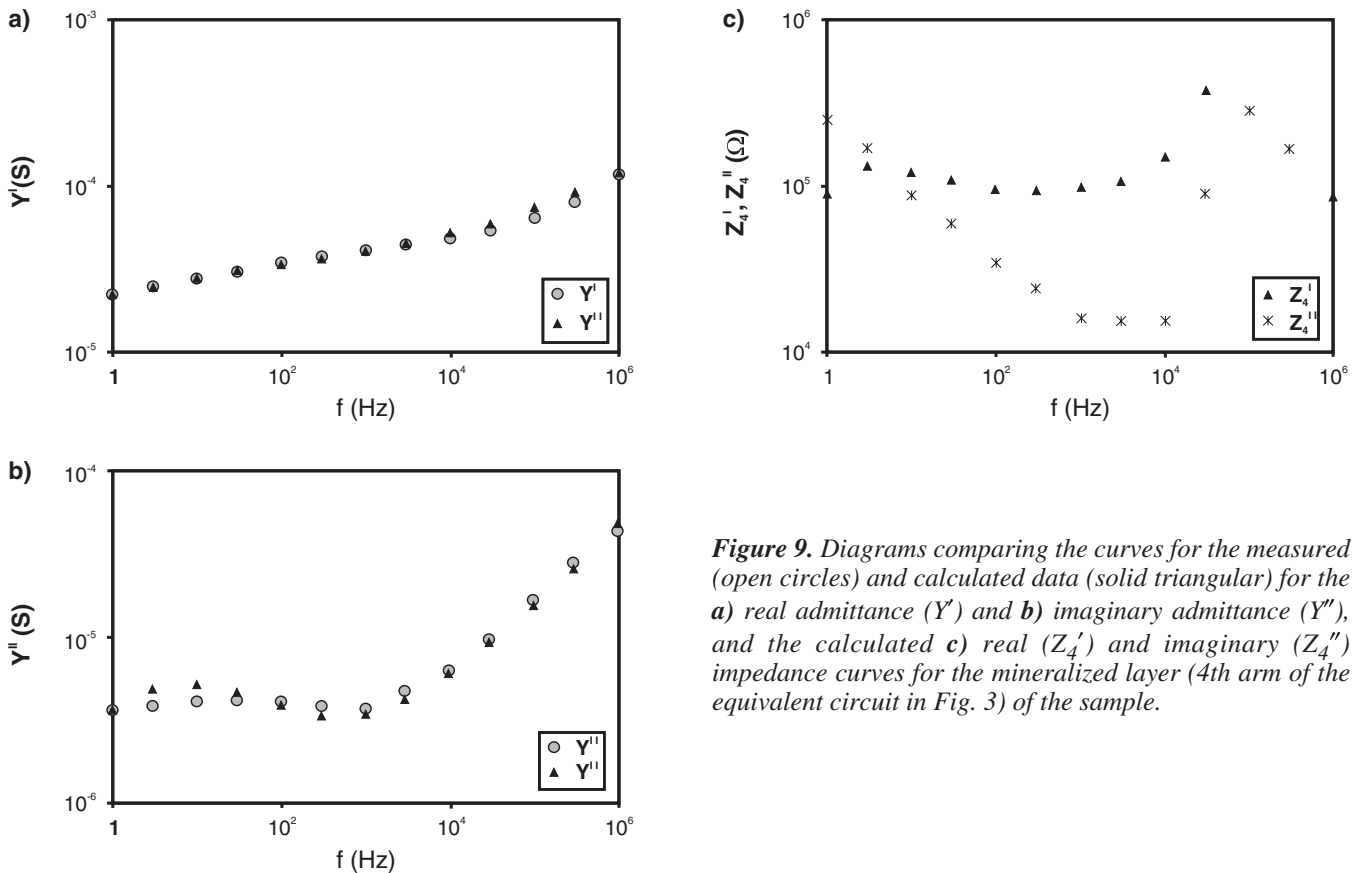


**Figure 9.** Diagrams comparing the curves for the measured (open circles) and calculated data (solid triangular) for the **a)** real admittance ( $Y'$ ) and **b)** imaginary admittance ( $Y''$ ), and the calculated **c)** real ( $Z_4'$ ) and imaginary ( $Z_4''$ ) impedance curves for the mineralized layer (4th arm of the equivalent circuit in Fig. 3) of the sample.

**Table 5.** Complex admittance data calculated from the equivalent circuit coefficients (Table 4) obtained by curve fitting of the measured complex admittance data in Table 3 and Figures 9a and 9b.

f	Y*(x10 <sup>-6</sup> )	Y'(x10 <sup>-6</sup> )	Y''(x10 <sup>-6</sup> )
1	23.5	23.1	3.88
3	25.8	25.3	4.91
10	29.0	28.6	5.28
30	32.0	31.6	4.78
10 <sup>2</sup>	34.9	34.7	3.92
3x10 <sup>2</sup>	37.7	37.5	3.43
10 <sup>3</sup>	41.5	41.3	3.51
3x10 <sup>3</sup>	46.1	45.9	4.30
10 <sup>4</sup>	53.3	52.9	6.22
3x10 <sup>4</sup>	62.6	61.9	9.45
10 <sup>5</sup>	77.4	75.7	15.8
3x10 <sup>5</sup>	97.2	93.6	26.3
10 <sup>6</sup>	131	121	49.4
Hz	S	S	S

### Curve fitting

Following the estimates of the initial values for the nine equivalent circuit coefficients, a new set of Y'-f and Y''-f curves were calculated by entering them into Equations (11) and (12) (Table 5). Minor adjustments of these estimated values were made by visual interactive comparison of the calculated and measured curves. That is, by varying the coefficient values to obtain the best fit of the two curves using visual judgement. The best curve fits are displayed in Figures 9a and 9b, with the solid triangular plots representing the calculated data points. The final coefficient values resulting from this process are listed in Table 4. The error ranges in the table indicate the ranges of freedom of variation these final estimated coefficients can have in order to maintain consistency with the related sections of the current calculated curves within 20% (Fig. 9a, b).

## DISCUSSION AND CONCLUSIONS

### Electrode effect

No problematic effects have been experienced during data analysis of this study, even though the electrode effects have not been eliminated.

### Evaluation of curve fitting

There exists an alternative curve fitting method to estimate C<sub>M</sub>, α<sub>M</sub>, and R<sub>M</sub>, that can be used to evaluate the previous estimates. The impedance of the fourth arm (Equation 6) of the equivalent circuit in Figure 3 can be expressed by

$$Z_4 = Z_4' - jZ_4'', \quad (39)$$

where

$$Z_4' = R_M, \quad (40)$$

$$Z_4'' = 1/(C_M \omega^{1-\alpha_M}). \quad (41)$$

Since six of the coefficients (C<sub>D</sub>, C<sub>S</sub>, α<sub>SC</sub>, R<sub>S</sub>, α<sub>SR</sub>, and R<sub>P</sub>) in Equations (11) and (12) are now known (Table 4), the real and imaginary admittances of the fourth arm, Y<sub>4</sub>' and Y<sub>4</sub>'', can be derived from the following equations:

$$Y_4' = Y' - \{1/R_P + 1/(R_S \omega^{-\alpha_{SR}})\}, \quad (42)$$

$$Y_4'' = Y'' - \{\omega C_D + C_S \omega^{1-\alpha_M}\}. \quad (43)$$

The Z<sub>4</sub>' and Z<sub>4</sub>'' can also be determined by the following equations:

$$Z_4' = Y' / (Y_4'^2 + Y_4''^2), \quad (44)$$

$$Z_4'' = Y'' / (Y_4'^2 + Y_4''^2). \quad (45)$$

The Z<sub>4</sub>' and Z<sub>4</sub>'' versus frequency (f) curves, derived from Equations (44) and (45), are displayed in Figure 9c. The Z<sub>4</sub>'-f curve that should be constant, according to Equation (40), is actually relatively flat in the 1–3000 Hz range with Z<sub>4</sub>' having an average value of 1.07x10<sup>5</sup> ± 0.27x10<sup>5</sup> Ω (±30%). The estimated value of 10<sup>5</sup> Ω (Table 4) from the previous curve fitting is within 10% of this average value, and therefore is consistent.

The Z<sub>4</sub>''-f curve shows a rapid decrease with increased frequency, as expected from Equation (41), to about 1000 Hz at which point it levels off. From the gradient of this curve, we obtain values of 1.7x10<sup>-6</sup>–2.4x10<sup>-6</sup> F for C<sub>M</sub> and 0.54–0.63 for α<sub>M</sub>. The estimated values of 1.95x10<sup>-5</sup> F and 0.596 (Table 4), from curve fitting, for these two coefficients are well within the range of these values.

### Characteristics of mineralized sericite

The results of the curve-fitting evaluation, the relatively good fit between the measured and calculated curves (Fig. 9a, b), and the reasonably small error ranges of the coefficients (Table 4) suggest that the equivalent circuit coefficient estimates are relatively good. The error ranges of the frequency coefficients (α<sub>SC</sub>, α<sub>SR</sub>, α<sub>M</sub>) are in the range of ±1% to ±12%, and those of the other coefficients are ±15% to ±50%. The error ranges of the latter set of coefficients are small, considering the fact that the values of these coefficients can vary over a range of many decades. These values must now be converted into values independent of sample volume and dimensions, in order to represent the electrical characteristics of the rock sample. This is accomplished by use of the geometric factor (K<sub>G</sub>), as follows:

$$\rho_X = R_X K_G, \quad (46)$$

for the resistivity (ρ<sub>X</sub>) and resistance (R<sub>X</sub>) parameters, and

$$\epsilon_X = C_X / K_G, \quad (47)$$

for the permittivity (ε<sub>X</sub>) and capacitance (C<sub>X</sub>) parameters in Table 4. The results of these conversions are compiled in Table 6.

**Table 6.** Bulk and fractional electrical characteristics of the electrically anisotropic sericite schist sample (MYG-11A), from the Yellowknife mining district, Northwest Territories.

Coefficients/parameters	Symbol	Obtained from	Bulk values	Fraction values	Units
Rock permittivity	$\epsilon_D$	$C_D$	$1.34 \times 10^{-10}$	$2.2 \times 10^{-10}$	F/m
Pore surface permittivity	$\epsilon_S$	$C_S$	$4.03 \times 10^{-6}$	$6.7 \times 10^{-6}$	F/m
Coefficient		$\alpha_{SC}$	0.59	0.59	
Pore surface resistivity	$\rho_S$	$R_S$	$1.79 \times 10^4$	$1.1 \times 10^4$	$\Omega \cdot m$
Coefficient		$\alpha_{SR}$	0.3	0.3	
Resistivity of nonmineralized layer	$\rho_P$	$R_P$	$7.45 \times 10^2$	$4.5 \times 10^2$	$\Omega \cdot m$
Permittivity of mineralized layer	$\epsilon_M$	$C_M$	$1.44 \times 10^{-4}$	$5.4 \times 10^{-4}$	F/m
Coefficient		$\alpha_M$	0.596	0.596	
Resistivity of mineralized layer	$\rho_M$	$R_M$	$1.49 \times 10^3$	$5.9 \times 10^2$	$\Omega \cdot m$

The sericite schist sample (MYG-11A) used in this study has a thickness of 1.51 cm in the direction perpendicular to the foliation (Fig. 5, Table 1). Of this the accumulated thickness of the mineralized layers ( $\ell_{MT}$  in Fig. 4) is only 0.6 cm. This implies that these converted values are only bulk values and the fraction values have still to be determined. Since the total thicknesses of the mineralized and nonmineralized layers are 0.6 cm and 0.91 cm, that is 0.24 times and 0.76 times the thickness of the sample, the fraction values are  $0.24\rho_X$  and  $\epsilon_X/0.24$  for the mineralized layers and  $0.76\rho_X$  and  $\epsilon_X/0.76$  for the nonmineralized layers. These results are also included in Table 6.

Results of this study indicate the existence of dielectric effects of the rock-forming minerals, frequency-dependent permittivity and resistivity effects of the pore surfaces in the layers barren of sulphide minerals, nonfrequency-dependent resistivity effects in both the mineralized and nonmineralized layers, and frequency-dependent permittivity effects of the electrochemical double layers on the sulphide grains in the mineralized layers. These effects have been characterized by using nine coefficients of an equivalent circuit to model the rock. These coefficients were determined by several methods, including interactive curve-fitting of calculated curves to the actual measured curves.

The sulphide mineral surface permittivity ( $\epsilon_M$ ) value of  $5.4 \times 10^{-4}$  F/m, obtained in this study, is in the same order of magnitude as those estimated from published data ( $10^{-4}$ – $10^{-6}$  F/m) for solid chalcopyrite and galena samples (Katsube, 1975b). This value, however, is likely somewhat smaller than the true values of these sulphide mineral surfaces. This is because it is a result of the electrical current flowing through multiple surfaces of fine-grained sulphides which is simulated by a multiple number of capacitances in series. Since the permittivity of vacuum ( $\epsilon_0$ ) is  $8.854 \times 10^{-12}$  F/m, the permittivity ( $\epsilon_D$ ) value of  $2.2 \times 10^{-10}$  F/m (Table 6) for our sample implies a relative dielectric constant ( $\kappa$ ) value of about 25. This is rather high for a rock and requires further investigation. We are not aware of any published information specifically related to the surface permittivity ( $\epsilon_S$ ) values. Information in a previous publication (Katsube, 1975c), however, implies  $\epsilon_D \ll \epsilon_S \ll \epsilon_M$ . The  $\epsilon_S$  value of  $6.7 \times 10^{-6}$  F/m for this study is somewhat consistent with that information. The  $\rho_P$  and  $\rho_M$  values of 400–600  $\Omega \cdot m$  for this study are within

the range of values for bulk electrical resistivity ( $\rho_R$ ) commonly observed for anisotropic rocks (e.g. Connell et al., 2000).

## ACKNOWLEDGMENTS

The author expresses his thanks to Y. Das (Defence Research Establishment Suffield, Alberta) for critically reviewing this paper and for his useful comments. The author also acknowledges S. Connell (GSC Ottawa) for her assistance in the analysis of part of the data used in this paper.

## REFERENCES

- Collett, L.S. and Katsube, T.J.**  
1973: Electrical parameters of rocks in developing geophysical techniques; *Geophysics*, v. 38, p. 76–91.
- Connell, S., Hunt, P., and Katsube, T.J.**  
2000: Electrical mechanism of sericite schists from Giant and Con mine areas, Northwest Territories; *in* Current Research 2000; Geological Survey of Canada, 7 p. (CD-ROM).
- Davis, J.C.**  
1986: *Statistics and Data Analysis in Geology*; John Wiley & Sons, New York, New York, p. 200–204.
- Dias, C.A.**  
1972: Analytical model for a polarizable medium at radio and lower frequencies; *Journal of Geophysical Research*, v. 77, p. 4945–4956.  
2000: Developments in a model to describe low-frequency electrical polarization of rocks; *Geophysics*, v. 65, p. 437–451.
- Gauvreau, C. and Katsube, T.J.**  
1975: Automation in electrical rock property measurements; *in* Current Research, Part A; Geological Survey of Canada, Paper 75-1A, p. 83–86.
- Katsube, T.J.**  
1975a: The critical frequency and its effect on EM propagation; *in* Current Research, Part A; Geological Survey of Canada, Paper 75-1A, p. 101–105.  
1975b: Frequency range for mineral differentiation by IP methods; *in* Current Research, Part A; Geological Survey of Canada, Paper 75-1A, p. 95–98.  
1975c: The electrical polarization mechanism model for moist rocks; *in* Current Research, Part C; Geological Survey of Canada, Paper 75-1C, p. 353–360.
- Katsube, T.J. and Collett, L.S.**  
1973: Electrical characteristics of Apollo 16 lunar samples; *Proceedings of Fourth Lunar Science Conference*, Pergamon Press, v. 3, p. 3101–3110.  
1975: Electromagnetic propagation characteristics of rocks; *in* The Physics and Chemistry of Rocks and Minerals, (ed.) R.G.J. Strens; John Wiley & Sons Ltd., London, United Kingdom, p. 279–295.

**Katsube, T.J. and Mareschal, M.**

1993: Petrophysical model of deep electrical conductors; Graphite lining as a source and its disconnection due to uplift; *Journal of Geophysical Research*, v. 98, no. B5, p. 8019–8030.

**Katsube, T.J. and Salisbury, M.**

1991: Petrophysical characteristics of surface core samples from the Sudbury structure; *in Current Research, Part E*; Geological Survey of Canada, Paper 91-E, p. 265–271.

**Katsube, T.J. and Walsh, J.B.**

1987: Effective aperture for fluid flow in microcracks; *International Journal of Rock Mechanics and Mining Sciences & Geomechanics Abstracts*, v. 24, p. 175–183.

**Madden, T.R. and Cantwell, T.**

1967: Induced polarization; A review; *in Mining Geophysics, Volume 2*; Society of Exploration Geophysics, p. 373–400.

**Pelton, W.H.**

1977: Interpretation of complex resistivity and dielectric data; Ph.D. thesis, University of Utah, Salt Lake City, Utah, 272 p.

**Pelton, W.H., Ward, S.H., Hallof, P.G., Sill, W.R., and Nelson, P.H.**

1978: Mineral discrimination and removal of inductive coupling with multifrequency IP; *Geophysics*, v. 43, no. 3, p. 588–609.

**Scromeda, N., Connell, S., and Katsube, T.J.**

2000: Petrophysical properties of mineralized and nonmineralized rocks from Giant and Con mine areas, Northwest Territories; *in Current Research 2000*; Geological Survey of Canada, 7 p. (CD-ROM).

**von Hippel, A.R.**

1954a: *Dielectrics and Waves*; John Wiley and Sons, Inc., New York, New York, 284 p.

1954b: *Dielectric Materials and Applications*; MIT Press, Cambridge, Massachusetts, 438 p.

**Wait, J.R.**

1959: A phenomenological theory of overvoltage for metallic particles; *in Overvoltage Research and Geophysical Applications*, (ed.) J.R. Wait; Pergamon Press, International Series on Earth Sciences, v. 4, p. 22–28.

**Ward, S.H. and Fraser, D.C.**

1967: Conduction of electricity in rocks; *in Mining Geophysics, Volume II*, Society of Exploration Geophysics, and *Mining Geophysics Volume II*, Society of Exploration Geophysics, Tulsa, Oklahoma, p. 197–223.

**Wong, J.**

1979: An electrochemical model of the induced polarization phenomena in disseminated sulphide ores; *Geophysics*, v. 44, p. 1245–1265.

**Zonge, K.L.**

1972: Electrical properties of rocks as applied to geophysical prospecting; Ph.D. thesis, University of Arizona, Tucson, Arizona, 156 p.

---

Geological Survey of Canada Project 870057